JPE 16-3-31

http://dx.doi.org/10.6113/JPE.2016.16.3.1141
ISSN(Print): 1598-2092 / ISSN(Online): 2093-4718

Novel Islanding Detection Method for Distributed PV Systems with Multi-Inverters

Dufeng Cao†, Yi Wang*, Zhenao Sun**, Yibo Wang**, and Honghua Xu**

†,*School of Electrical Engineering, Beijing Jiaotong University, Beijing, China
**Institute of Electrical Engineering, Chinese Academy of Sciences, Beijing, China

Abstract

This study proposes a novel islanding detection method for distributed photovoltaic (PV) systems with multi-inverters based on a combination of the power line carrier communication and Sandia frequency shift islanding detection methods. A parameter design method is provided for the novel scheme. On the basis of the designed parameters, the effect of frequency measurement errors and grid line impedance on the islanding detection performance of PV systems is analyzed. Experimental results show that the theoretical analysis is correct and that the novel method with the designed parameters has little effect on the power quality of the inverter output current. Non-detection zones are not observed, and a high degree of reliability is achieved. Moreover, the proposed islanding detection method is suitable for distributed PV systems with multi-inverters.

Key words: Distributed PV system, Islanding, Non-detection zone, Power quality

I. INTRODUCTION

Ongoing economic development ensures the constant depletion of conventional energy. In such a case, distributed photovoltaic (PV) systems are highly appealing as a power generation technique because they are energy efficient and environmentally friendly. One of the main challenges faced by distributed generation applications is the prevention of islanding. Islanding is a condition in which a portion of a utility system that contains both load and distributed resources remains energized while isolated from the remainder of the utility system [1]. Despite the low probability of unintentional islanding, it still poses a major safety risk to both maintenance personnel and electrical equipment. In addition, the non-synchronized phenomenon between the islanded part and the grid hinders the recovery of normal power supply. Therefore, islanding in distribution generation must be detected in a timely manner to improve the safety and reliability of distributed power generation systems and to protect people and equipment from safety hazards.

The main techniques for islanding detection are classified as remote and local [2]. Remote techniques are based on the communication between the grid and the distribution generation system; here, power line carrier communication (PLCC) is widely used [3]-[5]. Local techniques can be further divided into passive and active methods. The passive method utilizes inverter output voltage, frequency, phase, or harmonics variation to detect islanding. However, when a balance exists between the output power of the PV system and the local load power, the passive islanding detection method loses its detection ability; therefore, the non-detection zone (NDZ) is large. Typical passive methods include the over/under voltage and over/under frequency detection methods [6-7], voltage harmonic detection method [8], [9], and voltage phase jump detection method [10]. The active islanding detection method utilizes inverter control to produce a particular disturbance in output power, frequency, or phase. Once islanded, the disturbance of the inverter output rapidly accumulates, resulting in a parameter outside the permissible range; in such a case, islanding can be detected. Active islanding detection methods include active frequency drift [11], [12], slip mode frequency shift [13], [14], Sandia frequency shift (SFS) [15-16], GE anti-islanding [17], reactive power variation [18]-[20], and impedance measurements [21]-[23].

Manuscript received Nov. 2, 2015; accepted Feb. 21, 2016
Recommended for publication by Associate Editor Yujin Song.
†Corresponding Author: 12117366@bjtu.edu.cn
Tel: +86-18910761312, Beijing Jiaotong University
*School of Electrical Engineering, Beijing Jiaotong University, China
**Institute of Electrical Engineering, Chinese Academy of Sciences, China

Current research on islanding detection methods is mainly based on single inverter models. Hence, the effectiveness of these methods when a large number of inverters are connected to the grid is worth exploring. Previous studies have examined the effect of the number of inverters on the run-on time of islanding [24]. Other works have studied the effects of two different inverters (with the same and with different islanding detection methods) on anti-islanding protection performance [25], [26].

Although these methods achieve high precision and small NDZs, they reduce the power quality of the inverter output current. Furthermore, the different methods in the multi-inverter may interact with one another and invalidate the anti-islanding of the system. To improve the anti-islanding performance of multi-inverter systems, we propose a novel islanding detection method based on the PLCC and SFS methods. Although these two methods are not new, their combination produces a novel islanding detection method that has not been reported elsewhere. Experiments show that the new scheme performs significantly better than existing methods.

This paper is organized as follows. Section II describes the principles of the novel islanding detection method, introduces the carrier signal generator and detector, and provides the guidelines for the parameter design of the SFS method. Section III provides further analysis of the effect of frequency measurement errors and line impedance on the performance of the new scheme, with the designed parameters serving as basis of the analysis. Section IV provides the experiment results to verify the theoretical analysis results and the new scheme. Section V presents the conclusions.

II. New Islanding Detection Method

A. Carrier Signal Generator and Carrier Signal Detector

Fig. 1 shows the installation position of the carrier signal generator and signal detector. The signal generator of the PLCC program is connected to the secondary substation bus side, with a signal detector device installed beside each inverter. Fig. 2 shows the waveform of the carrier, which is transmitted in zero crossing of the sinusoidal voltage. The lower section shows the 220 V AC phase voltage with the carrier signal; the upper section shows the waveform of the carrier signal from the analytical device that is amplified 100 times.

The carrier signal involves three clusters of the high-frequency carrier in each half-cycle of the phase voltage (one large cluster and two small clusters). The amplitude of the large signal is approximately 6 mV and is useful for this phase. The two small ones exist as three-phase carrier couplings and are difficult to eliminate. However, the signal detector could only detect large signals using reasonable detection thresholds; therefore, the effect of the two small

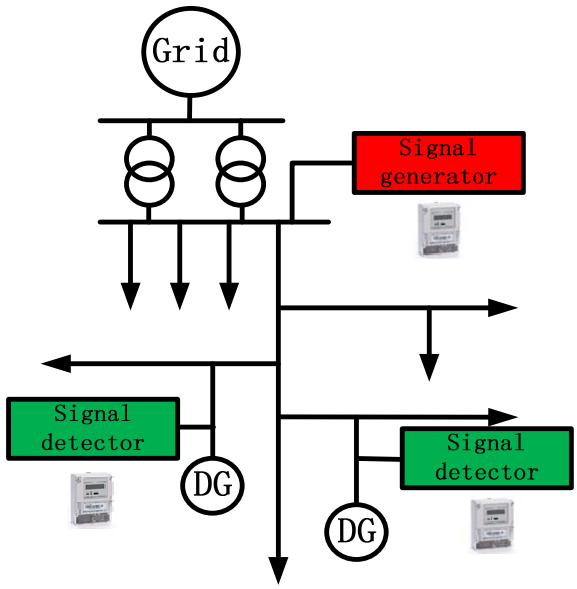

Fig.1. Distributed generation system.

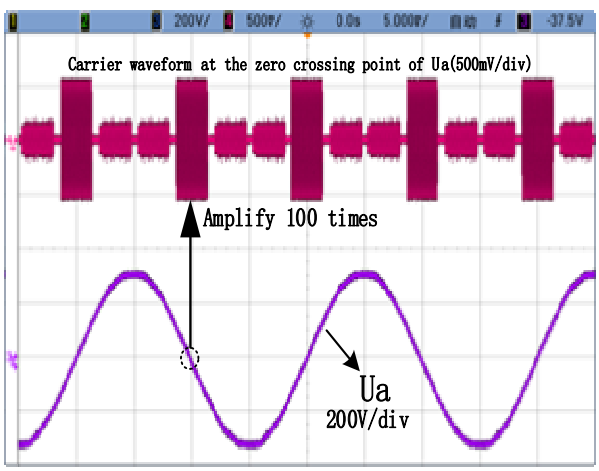

Fig. 2. Carrier signal in phase voltage.

signals is significantly reduced. Moreover, the effect of a high-frequency carrier with 6 mV amplitude on the power quality of a 220 V AC voltage can be ignored.

B. Principle of Novel Islanding Detection Method

Under typical operations, a signal generator continuously sends carrier signals through the grid line to all signal detectors, thus enabling the signal detector to detect the carrier and send a low-level trip signal to the inverter. In certain cases (e.g., breaker opening), the signal detector fails to receive carrier signals at a specific term; it thus sends a high-level trip signal to the inverter. When the inverter detects this high-level trip signal, the following occurs. The inverter does not immediately stop operating. The local SFS islanding detection method is performed in a timely manner, and the voltage frequency of the point of common coupling (PCC) is detected for the entire duration. If the frequency does not fall within 49.5–50.5 Hz, then the inverter

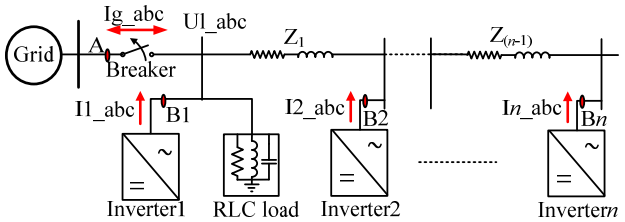

Fig. 3. Schematic diagram of the multi-inverter system.

immediately stops operating, thus indicating the detection of islanding. If the PCC voltage frequency falls within the allowable range, the inverter continues to operate. If the inverter receives a low-level trip signal from the detector during this 2 s period, it stops running the program (local SFS method). In the inverter operation, if the high-level trip signal lasts for more than 2 s, the inverter sends an alarm signal and displays PLCC failure, which triggers troubleshooting protocols for the maintenance personnel. Until the fault is cleared, the inverter does not stop running the local islanding detection method. The advantage here is that the novel islanding detection method benefits from the remote method not affecting the quality of the inverter output current and from the active method performing correctly. Therefore, the proposed method avoids the unreliability of the remote method and the prolonged effect on power quality of the active method.

C. Design Parameters of Sandia Frequency Shift Islanding Detection Method

PLCC only provides a signal to the inverter. A high-level trip signal means that the inverter may be islanding. The islanding detection performance of an inverter depends on the effectiveness of the SFS islanding detection method. Therefore, we present in this section the design parameters for the SFS method. The investigated system is shown in Fig. 3.

For simplification purposes, we assume that all the installed inverters in Fig. 3 are manufactured by the same firm and are of the same type. Hence, the rated powers of the inverters are deemed equal. The output current of the *j*-th inverter is assumed as

$$i_j = m_j \cdot I \cdot \sin(2\pi ft + \theta_j) \tag{1}$$

where f is the measurement frequency of each inverter, m_j is the ratio of the output power of inverter j to its rated power ($j = 1,2,\cdots,n$), and θ_j is the phase angle of the current i_j (introduced by the SFS method) and is written as

$$\theta_j = \frac{\pi}{2} \cdot [k_j \cdot (f - f_g) + cf_j] \tag{2}$$

where k_j and cf_j ($j = 1,2,\cdots,n$) are the positive feedback gain and chopping fraction of the SFS method, respectively, and f_g is the rated frequency of the grid voltage (50 Hz).

The total output current of *n* inverters is

$$\begin{aligned} i &= \sum_{j=1}^{n} [m_j \cdot I \cdot \sin(2\pi ft + \theta_j)] \\ &= m \cdot I \cdot \sin(2\pi ft + \theta) \end{aligned} \tag{3}$$

where

$$m = \sqrt{[\sum_{j=1}^{n} (m_j \cdot \sin\theta_j)]^2 + [\sum_{j=1}^{n} (m_j \cdot \cos\theta_j)]^2} \tag{4}$$

$$\theta = \arctan \frac{\sum_{j=1}^{n} (m_j \cdot \sin\theta_j)}{\sum_{j=1}^{n} (m_j \cdot \cos\theta_j)} \tag{5}$$

When θ_j is small, the following equations can be derived:

$$\sin\theta_j \approx \theta_j \tag{6}$$

$$\cos\theta_j \approx 1 \tag{7}$$

Then, Eq. (5) can be expressed as follows:

$$\theta = \arctan \frac{\sum_{j=1}^{n} (m_j \cdot \theta_j)}{\sum_{j=1}^{n} m_j} \tag{8}$$

As shown in Eq. (8), the total output current phase angle θ of *n* inverters is related not only to weight m_j but also to phase angle θ_j. If the system anti-islanding protection method is effective, then Eq. (9) must be satisfied such that

$$\frac{d\theta}{df}\Big|_{f=f_g} \geq \frac{d\theta_{load}}{df}\Big|_{f=f_g} \tag{9}$$

where

$$\theta_{load} = -\arctan[Q_f \cdot (\frac{f_0}{f} - \frac{f}{f_0})] \tag{10}$$

In Eq. (10), θ_{load} is the phase angle of the load current relative to its voltage, Q_f is the quality factor of the parallel RLC load, and f_0 is the resonant frequency of the parallel RLC load.

Eq. (11) can be derived from Eqs. (2), (8), (9), and (10).

$$\frac{\sum_{j=1}^{n} (m_j \cdot k_j)}{\sum_{j=1}^{n} m_j} \geq \frac{4 \cdot Q_f}{\pi \cdot f_0} \tag{11}$$

m_1, m_2,$\cdots$,m_n are different and may change during the operation of actual inverters. Hence, if Eq. (11) is maintained at any time, the most convenient and feasible method is to make the positive feedback gain k_j of the inverter equal, i.e., $k_1 = k_2 = \cdots = k_n = k$. Then, Eq. (11) can be simplified as follows:

$$k \geq \frac{4 \cdot Q_f}{\pi \cdot f_0} \tag{12}$$

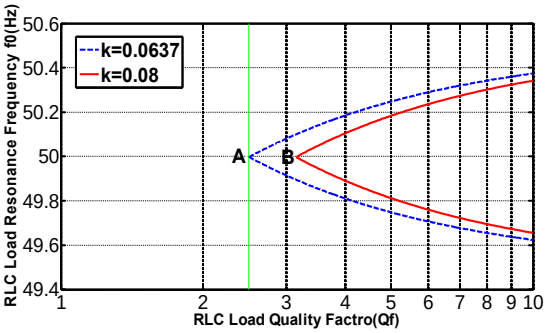

Fig. 4. NDZs of SFS method under different positive feedback gains.

As shown in Eq. (12), the anti-islanding protection of the system is not affected by weight m_j, i.e., by the actual output power of each inverter. Therefore, islanding detection in a multi-inverter system is the same as that in a single inverter unit. If the positive feedback gain k exceeds $\frac{4\cdot Q_f}{\pi\cdot f_0}$, then the multi-inverter system can effectively detect islanding. However, if the positive feedback gain becomes too large, then instability may occur despite the grid connection of the inverter [27]. When the value of Q_f is 2.5 and f_0 is 50 Hz, the value of $\frac{4\cdot Q_f}{\pi\cdot f_0}$ is approximately 0.0637.

During islanding, Eq. (13) can be derived according to the phase criterion ($\theta=\theta_{load}$) such that

$$\theta=-\arctan[Q_f\cdot(\frac{f_0}{f}-\frac{f}{f_0})] \tag{13}$$

Thus, Eq. (14) is

$$f_0^2+\frac{f\cdot\tan\theta}{Q_f}f_0-f^2=0 \tag{14}$$

By substituting $f_{\max}=50.5$ Hz and $f_{\min}=49.5$ Hz into Eq. (14) and replacing the frequency (f) with these frequency thresholds, we can obtain the NDZ boundary of the SFS method as

$$f_{0\max}=\frac{f_{\max}}{2Q_f}\{-\tan[\theta(f_{\max})]+\sqrt{\tan^2[\theta(f_{\max})]+4Q_f^2}\} \tag{15a}$$

$$f_{0\min}=\frac{f_{\min}}{2Q_f}\{-\tan[\theta(f_{\min})]+\sqrt{\tan^2[\theta(f_{\min})]+4Q_f^2}\} \tag{15b}$$

The resonant frequency is calculated by varying the value of Q_f in Eq. (15). The NDZ can now be plotted by applying Eq. (15). Fig. 4 shows the NDZs for different positive feedback gains in the $Q_f\times f_0$ load parameter space.

For a given positive feedback gain *k*, the NDZ indicates that the inverter(s) cannot detect islanding under certain load parameter (Q_f and f_0) conditions. In Fig. 4, the zone surrounded by a dotted line is the NDZ of the system for $k=0.0637$. Point A is the summit of the NDZ, and the straight line over point A is $Q_f=2.5$. If the RLC load quality factor Q_f is less than 2.5, then the system is able to detect islanding. According to the literature [28], in the left plane of line A, the islanded system becomes unstable after islanding. A low RLC load (Q_f) equates to a short islanding detection time. If the RLC load quality factor Q_f is equal to 2.5 and f_0 is equal to 50 Hz according to the NDZ in Fig. 4, then the system may detect islanding in this critical condition, but the NDZ is unable to reflect the islanding detection time. A previous study [29] showed that the islanding detection time may be longer than 2 s, which fails to meet standard requirements. Therefore, in our design of the positive feedback gain according to $k=\frac{4\cdot Q_f}{\pi\cdot f_0}$, we set the selective quality factor value Q_f to be slightly higher than 2.5 and recommend a value of approximately 3.15. The designed positive feedback gain *k* is 0.08. In Fig. 4, the zone surrounded by a solid line is the NDZ of the system for $k=0.08$. Fig. 4 shows that the positive feedback gain determines the strength of the SFS method for a multi-inverter system. A large gain equates to a small NDZ, that is, the anti-islanding scheme is effective. Hence, for $k=0.08$, the system can realize rapid islanding protection as long as the parallel RLC load quality factor (Q_f) is not greater than 2.5, which indicates no-NDZ. In this way, the standard requirements are met [1].

Chopping fraction is another parameter of the SFS method. According to the literature [11], the total harmonic distortion (THD) of the output current of the inverter is linear with cf_0. As such, cf_0 should not be greater than 0.05. In this work, cf_0 of each inverter is equal to 0.02.

According to the proposed design method, a multi-inverter grid-connected system can realize islanding detection despite the different capacities of inverters because θ_j ($j=1,2,\cdots,n$) is equal to θ. The current injected by *n* inverters is shown in Eq. (16).

$$\begin{aligned} i&=\sum_{j=1}^{n}[m_j\cdot I_j\cdot\sin(2\pi ft+\theta_j)]\\ &=\sin(2\pi ft+\theta)\cdot\sum_{j=1}^{n}[m_j\cdot I_j] \end{aligned} \tag{16}$$

Phase θ of the total current is clearly not related to the rated power and actual output power of each inverter. The islanding detection performance of a multi-inverter with different rated power levels is the same as that of a single

inverter system.

III. Effect of Frequency Measurement Errors and Line Impedance on the Performance of the Novel Scheme with Designed Parameters

A. Effect of Frequency Measurement Errors on the Performance of the Novel Scheme with Designed Parameters

This section explores the effect of frequency measurement errors on the overall islanding detection performance via mutual dilution of *n* inverters.

The measured frequency of the j-*th* inverter is assumed to be

$$f_j = f + \Delta f_j \tag{17}$$

where f is the actual frequency of the grid voltage and Δf_j is the frequency measurement error ($j = 1,2,\cdots,n$).

If the positive feedback gain of each inverter is the same ($k_1 = k_2 = \cdots = k_n = k$), then the initial chopping fraction is equal ($cf_1 = cf_2 = \cdots = cf_n = cf_0$). Eq. (18) can then be derived from Eq. (2).

$$\theta_j = \theta + \Delta\theta_j \tag{18}$$

where

$$\theta = \frac{\pi}{2} \cdot [k \cdot (f - f_g) + cf_0] \tag{19}$$

$$\Delta\theta_j = \frac{\pi}{2} \cdot k \cdot \Delta f_j \tag{20}$$

The total output current of *n* inverters is shown as

$$\begin{aligned} i &= \sum_{j=1}^{n} [m_j \cdot I \cdot \sin(2\pi f_j t + \theta_j)] \\ &\approx m \cdot I \cdot \sin(2\pi f t + \theta + \Delta\varphi) \end{aligned} \tag{21}$$

where

$$m = \sqrt{[\sum_{j=1}^{n}(m_j \cdot \sin\Delta\theta_j)]^2 + [\sum_{j=1}^{n}(m_j \cdot \cos\Delta\theta_j)]^2} \tag{22}$$

$$\Delta\varphi = \arctan\frac{\sum_{j=1}^{n}(m_j \cdot \sin\Delta\theta_j)}{\sum_{j=1}^{n}(m_j \cdot \cos\Delta\theta_j)} \tag{23}$$

When $\Delta\theta_j$ is small, Eq. (24) can be derived from Eq. (23).

$$\Delta\varphi = \arctan\frac{\sum_{j=1}^{n}(m_j \cdot \Delta\theta_j)}{\sum_{j=1}^{n} m_j} \tag{24}$$

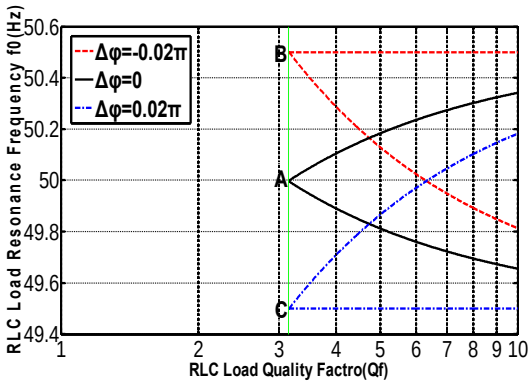

Fig. 5. Effect of frequency measurement errors on NDZ.

The NDZ boundary in Eq. (25) is obtained from Eq. (21) and the phase criterion.

$$\begin{aligned} f_{r\max} = \frac{f_{\max}}{2Q_f}\{&-\tan[\theta(f_{\max}) + \Delta\varphi] \\ &+ \sqrt{\tan^2[\theta(f_{\max}) + \Delta\varphi] + 4Q_f^2}\} \end{aligned} \tag{25a}$$

$$\begin{aligned} f_{r\min} = \frac{f_{\min}}{2Q_f}\{&-\tan[\theta(f_{\min}) + \Delta\varphi] \\ &+ \sqrt{\tan^2[\theta(f_{\min}) + \Delta\varphi] + 4Q_f^2}\} \end{aligned} \tag{25b}$$

As shown in Eqs. (25), (24), and (20), the NDZ is related to Δf_j ($j = 1,2,\cdots,n$). As a worst case scenario for Δf_j with a relatively large value of 0.5 Hz, $\Delta\theta_j = \pm 0.02\pi$ if $k = 0.08$. The frequency measurement errors of *l* inverters are positive, and the frequency measurement errors of *n-l* inverters are negative. Eq. (26) can be derived from Eq. (24).

$$\Delta\varphi = \arctan[\frac{\sum_{j=1}^{l} m_j - \sum_{j=l+1}^{n} m_j}{\sum_{j=1}^{n} m_j} \cdot 0.02\pi] \tag{26}$$

Inequality $-0.02\pi < \Delta\varphi < 0.02\pi$ can be derived by analyzing Eq. (26). In Fig. 5, the NDZs can be plotted with Eq. (25), which is subject to $\Delta\varphi = -0.02\pi$, $\Delta\varphi = 0$, and $\Delta\varphi = 0.02\pi$.

Fig. 5 shows that frequency measurement errors change the shape of the NDZ of the *n* inverter system. When $\Delta\varphi = 0$, the NDZ of the multi-inverter system is the same as that in the ideal case (no frequency measurement errors). However, in the case of many inverters whose frequency measurement errors are positive and whose output powers are large, $\Delta\varphi$ is positive, point A moves vertically downward, and point C is the lower limit point. In the case of many inverters whose frequency measurement errors are negative and whose output powers are large, $\Delta\varphi$ is negative, point A moves vertically upward, and point B is the upper limit point. As long as $\Delta\varphi$ is not equal to zero, the NDZ shape is no longer symmetrical around 50 Hz. However, the NDZ does not

move in the horizontal direction, and the vertical line over points A, B, and C is $Q_f = 3.15$. If the RLC load quality factor Q_f does not exceed 2.5, then the system is deemed to achieve a perfect detection of islanding. This result means that frequency measurement errors do not result in the failure of the novel islanding detection method. Therefore, the islanding detection performance of the system is not substantially affected by frequency measurement errors.

B. Effect of Line Impedance on the Performance of the Novel Scheme with Designed Parameters

As described previously, frequency measurement errors of *n* inverters do not affect the islanding detection performance of the system. Therefore, for simplification, the measured frequencies of *n* inverters are assumed to be the same as the actual grid frequency.

Fig. 3 shows a line impedance between each pair of adjacent inverters; hence, the voltage phase of the PCC of each inverter may be different. The voltage phase difference of the PCC between the j-*th* inverter and the first inverter is assumed to be δ_j. The output current of the j-*th* inverter is

$$i_j = m_j \cdot I \cdot \sin(2\pi ft + \theta + \delta_j) \tag{27}$$

Then, the total output current of the inverters is

$$\begin{aligned} i &= \sum_{j=1}^{n} [m_j \cdot I \cdot \sin(2\pi ft + \theta + \delta_j)] \\ &= m \cdot I \cdot \sin(2\pi ft + \theta + \Delta\delta) \end{aligned} \tag{28}$$

where

$$m = \sqrt{[\sum_{j=1}^{n}(m_j \cdot \sin\delta_j)]^2 + [\sum_{j=1}^{n}(m_j \cdot \cos\delta_j)]^2} \tag{29}$$

$$\Delta\delta = \arctan\frac{\sum_{j=1}^{n}(m_j \cdot \sin\delta_j)}{\sum_{j=1}^{n}(m_j \cdot \cos\delta_j)} \tag{30}$$

Eq. (31) shows that the NDZ boundary can be obtained from Eq. (28) and the phase criterion.

$$f_{r\max} = \frac{f_{\max}}{2Q_f}\{-\tan[\theta(f_{\max}) + \Delta\delta] + \sqrt{\tan^2[\theta(f_{\max}) + \Delta\delta] + 4Q_f^2}\} \tag{31a}$$

$$f_{r\min} = \frac{f_{\min}}{2Q_f}\{-\tan[\theta(f_{\min}) + \Delta\delta] + \sqrt{\tan^2[\theta(f_{\min}) + \Delta\delta] + 4Q_f^2}\} \tag{31b}$$

As indicated in Eq. (30), we can obtain the inequality $\min(\delta_j) < \Delta\delta < \max(\delta_j)$. If $k = 0.08$, then the NDZs under different δ (Fig. 6) can be obtained according to Eq. (31). The values of δ are $0°$, $5°$, and $-5°$.

Fig. 6 shows that the voltage phase difference (δ) caused by line impedance only changes the shape of the NDZ.

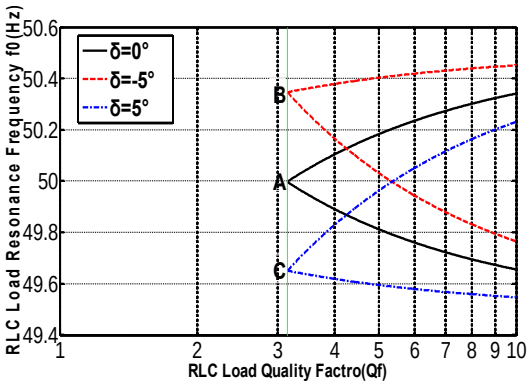

Fig. 6. Effect of phase angle error (δ) caused by line impedance on NDZ.

When δ is positive and increasing, the NDZ moves from point A toward point C along the vertical line. When δ is negative and decreasing, the NDZ moves from point A toward point B along the vertical line. $Q_f = 3.15$ denotes a straight line. For the parallel RLC load with $Q_f \le 2.5$, no NDZ forms with the use of the novel method with the designed parameters. Hence, the voltage phase error (δ) does not affect the novel islanding detection performance, i.e., line impedance exerts no influence on novel islanding detection performance.

IV. Experimental Results

Fig. 7 illustrates the experimental setup. The setup included three 10 kVA three-phase inverters, one variable line impedance cabinet, RLC load, and other components. Each inverter was controlled with a TMS320LF28335 digital signal processor (Texas Instruments). An FS75R12KT3 power module (Infineon) was used as the switching component. The device driver was an M57962 chip. The other main inverter components included a filter inductance of 1.5 mH, a filter capacitor of 66 μF, and step-up transformers with Δ/Y-type windings.

During testing, the DC power was supplied by a TOPCON 32 kW solar panel simulator. The main test equipment included a DL850 ScopeCorder and an HIOKI3196 power quality analyzer.

The test conditions were as follows: DC voltage of 380 V, rated AC voltage of 380 V, and a voltage frequency of 50 Hz. The active power of the RLC load was regulated to match the total output power of the inverters, and the quality factor Q_f was equal to 2.5.

For the test waveforms, the meaning of each symbol is as follows: I1_a is the phase A current of inverter 1, I2_a is the phase A current of inverter 2, Ul_abc is the three-phase AC voltage of the parallel RLC load, TS_1 is the trip signal from the signal detector to inverter 1, TS_2 is the trip signal from the signal detector to inverter 2, and Ig_abc is the current

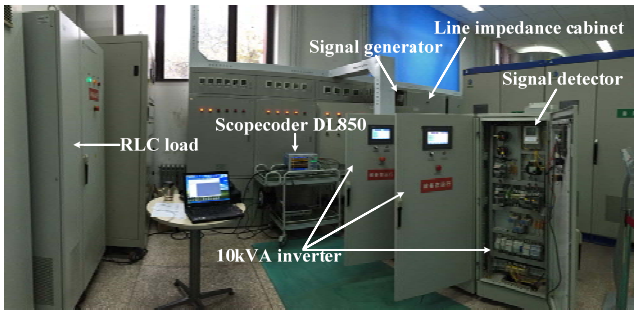

Fig. 7. Islanding experimental setup.

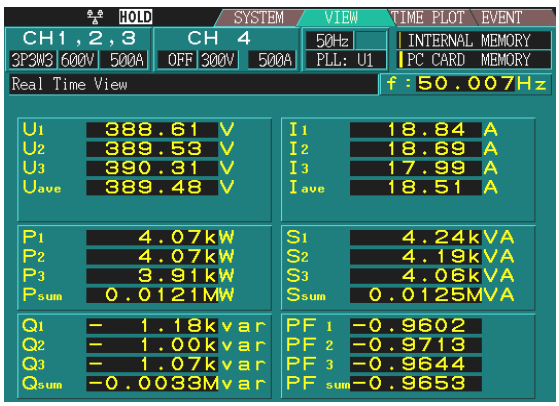

(a) Total output power and power factor.

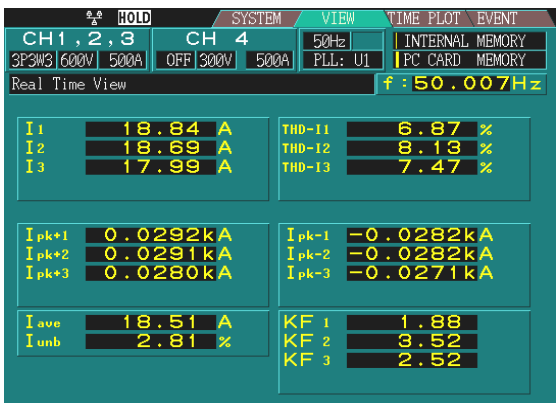

(b) THD of total output current.

Fig. 8. Output power, power factor, and current THD of the system under the SFS method.

between the multi-inverter system and the grid.

Fig. 8 shows the output power, power factor, and current THD of the system using only the SFS method. Fig. 9 shows the output power, power factor, and current THD of the system with the novel method. The results showed that the THD was smaller under the proposed method than under the SFS method. Furthermore, the power factor increased from 0.9602, 0.9713, and 0.9644 to 0.9896, 0.9798, and 0.9808, respectively. Therefore, unlike the SFS method, the novel method had little effect on the power quality of the inverter output current. We should note that the actual frequency of the power system was very close to 50 Hz. The proposed method could offer significant advantages over the SFS

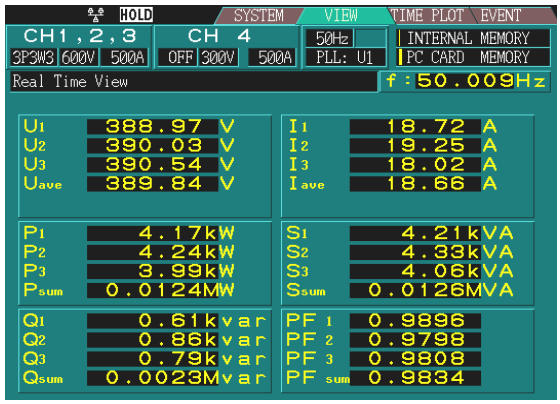

(a) Total output power and power factor.

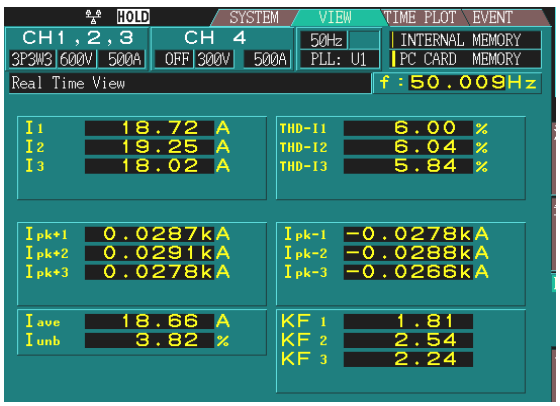

(b) THD of total output current.

Fig. 9. Output power, power factor, and current THD of the system under the novel method.

method should a grid simulator be able to set the actual frequency to values greater than 50 Hz, such as 50.4 or 49.6 Hz.

Fig. 10(a) shows the experimental waveform of the PLCC. When the inverters were under a grid-connected operation, the output power matched the load power. Hence, the grid current Ig_abc was extremely small. However, this condition did not imply islanding because the breaker was not disconnected (the grid current was not equal to zero). However, for some reason, e.g., a fault in the power supply of the signal generator, the signal detector sent a high-level trip signal to the inverter. The inverter immediately stopped running, and the output current dropped to zero. At the same time, the grid current suddenly increased because the grid supplied the load power. The fact that the inverters were tripped was deemed a nuisance and an indication of the unreliability of the PLCC. Fig. 10(b) shows the result of the novel method. Although the signal detector sent a high-level trip signal, the inverters did not immediately stop. The inverters initiated the SFS islanding protection method instead and constantly monitored the frequency of the PCC voltage. The inverter continued to run and provide power to the load because the frequency was held by the grid. Thus, the new method was significantly more reliable than the

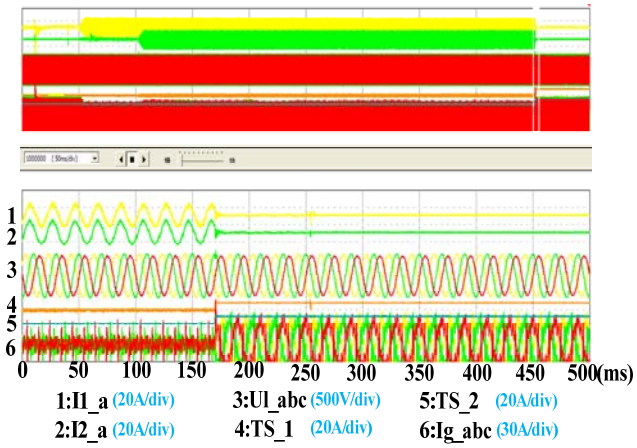

(a) Power line carrier communication.

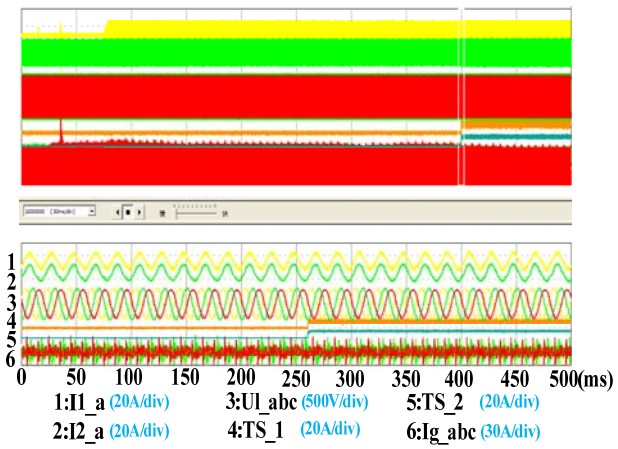

(b) Novel method.

Fig. 10. Comparison of power line carrier communication and novel islanding detection methods.

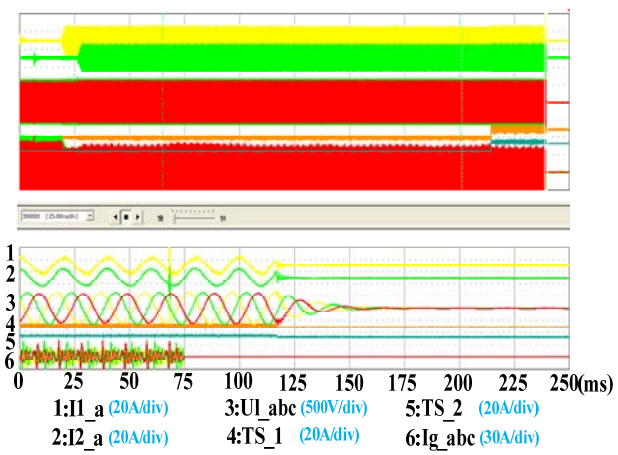

Fig. 11. Experimental results of the novel method under faulty PLCC conditions.

PLCC method. Fig. 11 shows the experiment using the novel method under a faulty PLCC. The inverters continued to operate despite the high trip signal. After a certain period, the system entered the islanding state, and the inverters stopped operating because of the SFS method. The islanding detection time was about 50 ms. This result further proves that the

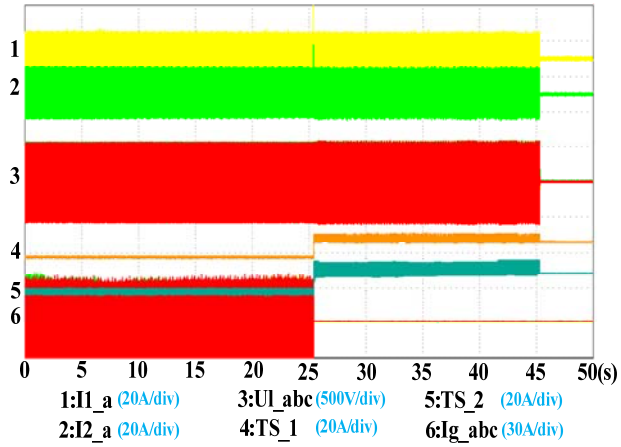

(a) Novel scheme ($k = 0.0637$)

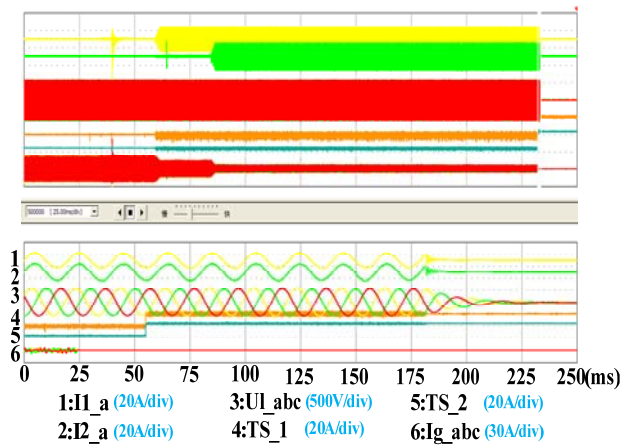

(b) Novel scheme ($k = 0.08$)

Fig. 12. Experimental results of the novel method under different positive feedback gains.

novel method is superior to the PLCC method.

Fig. 12 shows the experimental results of the novel method under islanding. No impedance can be observed between the two inverters. The experiment result for the case in which the positive feedback gain of the two inverters is equal to 0.0637 is shown in Fig. 12(a). Once islanded, the system could achieve islanding protection, with the islanding protection time being approximately 20 s. Such length of time clearly exceeded the standard of 2 s. The experiment result for the case in which the positive feedback gain of two inverters is equal to 0.08 is shown in Fig. 12(b). Islanding was clearly detected after approximately 160 ms, which satisfies the relevant standards. With the designed parameters ($k = 0.08$ and $cf_0 = 0.02$), the novel method can detect islanding rapidly and with a high degree of reliability. These two cases show the importance of the parameter design of the SFS method and prove that the proposed design is reasonable. They also indicate the correctness of the theoretical analysis.

When the frequency measurement error of inverter 1 was a positive 0.5 Hz, the frequency measurement error of inverter 2 was a negative 0.5 Hz. Moreover, the inverter output

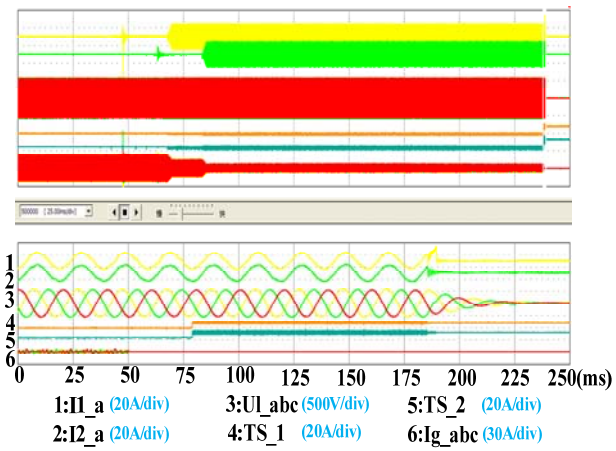

(a) Novel scheme ($\Delta f_1 = 0.5$, $\Delta f_2 = -0.5$, $\Delta\varphi = 0$).

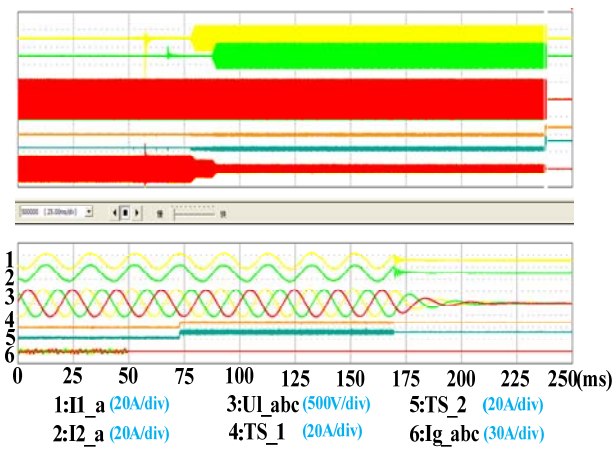

(b) Novel scheme ($\Delta f_1 = 0.5$, $\Delta f_2 = 0.5$, $\Delta\varphi = 0.02\pi$).

Fig. 13. Islanding result of the novel method under frequency measurement errors.

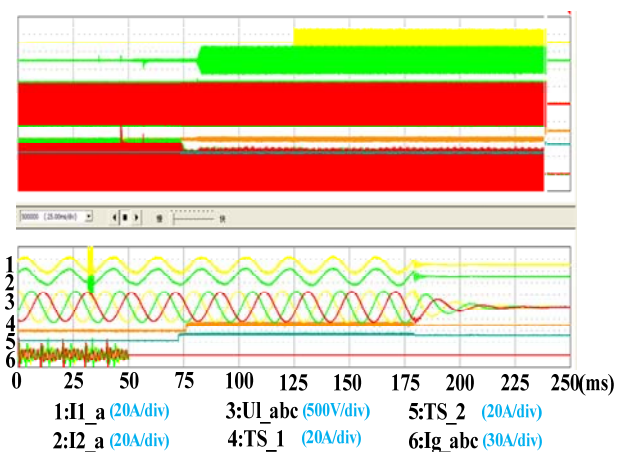

Fig. 14. Results of the novel method under two inverters ($L = 1.28$ mH).

power levels were equal, and $\Delta\varphi = 0$. When the frequency measurement errors of inverter 1 and inverter 2 were a positive 0.5 Hz, $\Delta\varphi = 0.02\pi$. Once islanded, islanding protection was realized (Fig. 13) with a detection time of approximately 150 and 125 ms. This case indicates that the theoretical analysis was correct and that the frequency measurement error did not affect the performance of the novel method with the proposed parameters.

The experiment result for the case in which an inductance of 1.28 mH exists between two inverters is shown in Fig. 14. Once islanded, the system could detect islanding, with the islanding detection time being approximately 135 ms, which satisfies the relevant standards. This case shows that even with impedance, the novel islanding detection method remained reliable and valid. This outcome is consistent with the analysis in Section III-B. The proposed method is clearly suitable for distributed PV generation.

V. Conclusion

This study investigated islanding detection in a distributed PV generation system. The following contributions were made.

A. This work proposes a novel islanding detection method that is suitable for the islanding protection of multi-inverter distributed systems. This work also provides parameter design guidelines for the SFS method.

B. Under the proposed parameter design, the novel method showed no NDZ. Furthermore, the results demonstrated that the frequency measurement errors and line impedance did not adversely affect the effectiveness of the novel scheme with the designed parameters.

C. The experimental results showed that the proposed scheme was able detect islanding in a timely manner and with a high degree of reliability; moreover, it had no adverse effect on power quality.

Acknowledgment

This work was supported by the National High Tech Research and Development Program (2015AA050402), Science and Technology Support Program (2015-GX-101A).

References

[1] IEEE Recommended Practice for Utility Interface of Photovoltaid (PV) Systems, IEEE Std. 929-2000, 2000.

[2] J. Yin, L. C. Chang, and C. Diduch, “Recent developments in islanding detection for distributed power generation,” in *Conf. LESCOPE-04*, pp. 124-128, 2004.

[3] W. Xu, G. Zhang, C. Li, W. Wang, G. Wang, and J. Kliber, “A power line signaling based technique for anti-islanding protection of distributed generators – Part I: scheme and analysis,” *IEEE Trans. Power De.*, Vol. 22, No. 3, pp. 1758-1766, Jul. 2007.

[4] W. Wang, J. Kliber, G. Zhang, W. Xu, B. Howell, and T. Palladino, “A power line signaling based scheme for anti-islanding protection of distributed generators – Part II: field test results,” *IEEE Trans. Power Del.*, Vol. 22, No. 3, pp. 1767-1772, Jul. 2007.

[5] M. Ropp, K. Aaker, J. Haigh, and N. Sabbah, "Using power line carrier communications to prevent islanding," in *Proc. 28th IEEE Photovoltaic Specialists Conference*, pp. 1675-1678, 2000.
[6] K. Tunlasakun, K. Kirtikara, S. Thepa, and V. Monyakul, "CPLD-based islanding detection for mini grid connected inverter in renewable energy," *IEEE TENCON*, Vol. 4, pp. 175-178, 2004.
[7] W. Freitas, W. Xu, C. M. Affonso, and Z. Huang, "Comparative analysis between ROCOF and vector surge relays for distributed generation applications," *IEEE Trans. Power Del.*, Vol. 20, No. 2, pp. 1315-1324, Apr. 2005.
[8] S. I. Jang and K. H. Kim, "An islanding detection method for distributed generations using voltage unbalance and total harmonic distortion of current," *IEEE Trans. Power Delivery*, Vol. 19, No. 2, pp. 745-752, Apr. 2004.
[9] V. Menon and M. H. Nehrir, "A hybrid islanding detection technique using voltage unbalance and frequency set point," *IEEE Trans. Power Syst.,* Vol. 22, No. 1, pp. 442-448, Feb. 2007.
[10] B. Singam and L. Y. Hui, "Assessing SMS and PJD schemes of anti-islanding with varying quality factor," *IEEE Power and Energy Conference*, pp. 196-201, Nov. 2006.
[11] M. E. Ropp, M. Begovic, and A. Rohatgi, "Analysis and performance assessment of the active frequency drift method of islanding prevention," *IEEE Trans. Energy Conversion*, Vol. 14, No. 3, pp. 810-816, Sep. 1999.
[12] H. L. Sun, "Performance assessment of active frequency drifting islanding detection methods," M.S. Thesis, Concordia University, Canada, 2005.
[13] W. Bower and M. Ropp, "Evaluation of islanding detection methods for photovoltaic utility-interactive power systems," Report IEA PVPS T5-09, 2002.
[14] G. A. Smith, P. A. Onions, D. G. and Infield, "Predicting islanding operation of grid connected PV inverters," *Electric Power Applications, IEE Proceedings,* Vol. 147, No. 1, pp. 1-6, 2000.
[15] M. Ropp, M. Begovic, A. Rohatgi, G. A. Kern, R. H. Bonn and S. Gonzalez, "Determining the relative effectiveness of islanding detection methods using phase criteria and non detection zones," *IEEE Trans. Energy Convers.*, Vol. 15, No. 3, pp. 290-296, Sep. 2000.
[16] V. John, Z. H. Ye, and A. Kolwalkar, "Investigation of anti-islanding protection of power converter based distributed generators using frequency domain analysis," *IEEE Trans. Power Electron.*, Vol. 19, No. 5, pp. 1177-1183, Sep. 2004.
[17] Z. Ye, R. Walling, L. Garces, R. Zhou, L. Li, and T. Wang, "Study and development of anti-islanding control for grid-connected inverters," National Renewable Energy Laboratory, 2004.
[18] G. H. Choe, H. S. Kim, H. G. Kim, Y. H. Choi, and J. C. Kim, "The characteristic analysis of grid frequency variation under islanding mode for utility interactive PV system with reactive power variation scheme for anti-islanding," *PESC 2006*, pp. 1-5, 2006.
[19] J. Zhang, D. H. Xu, G. H. Shen, Y. Zhu, N. He, and J. Ma, "An improved islanding detection method for a grid-connected inverter with intermittent bilateral reactive power variation," *IEEE Trans. Power Electron.*, Vol. 28, No. 1, pp. 268-278, Jan. 2013.
[20] Y. Zhu, D. Xu, N. He, J. Ma, J. Zhang, Y. Zhang, G. Shen, and C. Hu, "A novel RPV (reactive-power-variation) anti-islanding method based on adapted reactive power perturbation," *IEEE Trans. Power Electron.*, Vol. 28, No. 11, pp. 4998-5012, Nov. 2013.
[21] M. Liserre, F. Blaagjerg, and R. Teodorescu, "Grid impedance detection via excitation of LCL-filter resonance," *IEEE Industry Applications Conference*, Vol. 2, pp. 910-916, 2005.
[22] M. Ropp, J. Ginn, J. Stevens, W. Bower, and S. Gonzalez, "Simulation and experimental study of the impedance detection anti-islanding method in the single-inverter case," *IEEE Photovoltaic Energy Conversion Conference*, Vol. 2, pp. 2379-2382, 2006.
[23] F. Bertling and S. Soter, "A novel converter integratable impedance measuring method for islanding detection in grids with widespread use of decentral generation," *SPEEDAM*, pp. 503-507, 2006.
[24] D. Schutz and M. Ropp, "Simulation and experimental study of multi-inverter islanding," *Power and Energy Society General Meeting*, pp. 1-4, 2011.
[25] E. J. Estébanez, V. M. Moreno, A. Pigazo, M. Liserre, and A. Dell'Aquila, "Performance evaluation of active islanding-detection algorithms in distributed-generation photovoltaic systems: Two inverters case," *IEEE Trans. Ind. Electron*., Vol. 58, No. 4, pp. 1185-1193, Apr. 2011.
[26] L. A. C. Lopes and Y. Z. Zhang, "Islanding detection assessment of multi-inverter systems with active frequency drifting methods," *IEEE Trans. Power Del.*, Vol. 23, No. 1, pp. 480-486, Jan. 2008.
[27] X. Y. Wang, W. Freitas, V. Dinavahi, and W. Xu, "Investigation of positive feedback anti-islanding control for multiple inverter-based distributed generators," *IEEE Trans. Power Syst.*, Vol. 24, No. 2, pp. 785-795, May 2009.
[28] X. Y. Wang, W. Freitas, and W. Xu, "Dynamic non-detection zones of positive feedback anti-islanding methods for inverter-based distributed generators," *IEEE Trans. Power Del.*, Vol. 26, No. 2, pp. 1145-1155, Apr. 2011.
[29] Standard for Interconnecting Distributed Resources With Electric Power Systems, IEEE Std. 1547-2003, 2003.

Dufeng Cao received his B.S. and M.S. degrees from the School of Electrical Engineering of Beijing Jiaotong University, Beijing, China, in 1997 and 2008, respectively. Currently, he is pursuing his Ph.D. degree in Beijing Jiaotong University. His research interests include the control technology of grid-connected inverters and the impact of distributed generation on power quality.

Yi Wang was born in Liaoning, China, in 1958. He received his Ph.D. degree in Electrical Engineering from Xi'an Jiaotong University, Shanxi, China, in 1989. His research interests include new technology in high-voltage engineering, intelligent electrical appliances, partial discharge, and others. He is currently a Professor in the School of Electrical Engineering in Beijing Jiaotong University.

Zhenao Sun was born in Liaoning, China, in 1988. He received his B.S. degree from the School of Electrical Engineering of Beijing Jiaotong University in 2011. He is currently working toward his Ph.D. degree in the Institute of Electrical Engineering, Chinese Academy of Sciences. His research interests include the power quality of DG systems.

Yibo Wang received his Ph.D. degree from the University of the Chinese Academy of Sciences in 2009. Since 2014, he has been a Professor in the Institute of Electrical Engineering, Chinese Academy of Sciences. His current research interests include PV generation and the relationship of PV systems and power systems.

Honghua Xu received his B.S. and M.S. degrees from Tianjin University in 1985 and 1988, respectively. Since 1999, he has been a Professor in the Institute of Electrical Engineering, Chinese Academy of Sciences. His current research interests include PV generation, wind power generation, and power electronic technology.